Ab initio theory of gate induced gaps in graphene bilayers

Hongki Min,[1,*] Bhagawan Sahu,[2] Sanjay K. Banerjee,[2] and A. H. MacDonald[1]

[1]*Department of Physics, The University of Texas at Austin, Austin, Texas 78712, USA*
[2]*Microelectronics Research Center, The University of Texas at Austin, Austin, Texas 78758, USA*
(Received 9 December 2006; published 25 April 2007)

We study the gate-voltage induced gap that occurs in graphene bilayers using *ab initio* density functional theory. Our calculations confirm the qualitative picture suggested by phenomenological tight-binding and continuum models. We discuss enhanced screening of the external interlayer potential at small gate voltages, which is more pronounced in the *ab initio* calculations, and quantify the role of crystalline inhomogeneity using a tight-binding model self-consistent Hartree calculation.

I. INTRODUCTION

Recently, ultrathin graphite films including monolayers[1–3] and bilayers[4,5] have attracted considerable attention because of their novel properties. In single-layer graphene, the A sublattice to B sublattice hopping amplitude vanishes at two inequivalent points K and K' on the edge of the honeycomb lattice Brillouin zone (BZ); away from these points, the hopping amplitude grows linearly with the wave vector and has a phase which winds along with the orientation of the wave vector measured from the high-symmetry points. The band structure of an isolated graphene layer is therefore described at low energies by a two-dimensional massless Dirac equation with linear dispersion; this property gives rise to a half integer quantum Hall effect[6,7] and to a quantized spin Hall effect[8,9] and dominates the low-energy physics.

In bilayer graphene, the Bernal ($\widetilde{A}$-B) stacking illustrated in Fig. 1 modifies this electronic structure in an interesting way.[4,10] At K and K', the states localized at the $\widetilde{A}$ and B sites, are repelled from zero energy by interlayer tunneling; only states localized at A and $\widetilde{B}$ are present at zero energy. When tunneling is included, the A to $\widetilde{B}$ hopping is a second-order process via a virtual bonding or antibonding state at $\widetilde{A}$ and B. The chirality of the low-energy bands is therefore doubled. Most intriguingly, an external potential which induces a difference between the A and $\widetilde{B}$ site energies will open up a gap[11,12] in the spectrum. Band gaps controlled by applying a gate bias have been studied experimentally using angle-resolved photoemission spectroscopy[5] and Shubnikov–de Haas analysis[13] of magnetotransport. This unique property of bilayer graphene has created considerable interest in part because it suggests the possibility of switching the conductance of a graphene bilayer channel over a wide range at a speed which is limited by gate-voltage switching, as illustrated schematically in Fig. 2.

In this paper, we report on an *ab initio* density functional theory (DFT) study of the influence of an external potential difference between the layers on the electronic structure of a graphene bilayer. We compare our results with the phenomenological tight-binding and continuum model Schrödinger-Poisson calculations used in previous theoretical analyses.[12] DFT predicts, in agreement with these works, that the external potential difference is strongly screened with a maximum energy gap value of ∼0.3 eV. There are, however, quantitative differences. In particular, the enhanced screening which occurs for weak external potentials is stronger in the DFT calculations. In an effort to improve the quantitative agreement, we have estimated the influence of crystalline inhomogeneity in a tight-binding model self-consistent Hartree calculation. This effect strengthens intralayer Coulomb interactions because the charge is spatially bunched, and therefore increases screening in a Hartree calculation, but does not fully account for differences between the two calculations.

II. *AB INITIO* DENSITY FUNCTIONAL THEORY CALCULATIONS

We have performed *ab initio* DFT calculations[14] for an isolated graphene bilayer under a perpendicular external electric field using an all-electron linearized augmented plane wave plus local-orbital method incorporated in WIEN2K.[15] We used the generalized-gradient approximation[16] for the exchange and correlation potential.

A. External electric fields

To investigate the influence of an external electric field on a graphene bilayer, a periodic zigzag potential was applied along the z direction, perpendicular to the graphene planes, in a supercell.[17] The bilayer was placed at the center of the constant external electric field region and the size of the supercell was set to a large value (∼16 Å) to minimize the interaction between bilayers in neighboring supercells. In or-
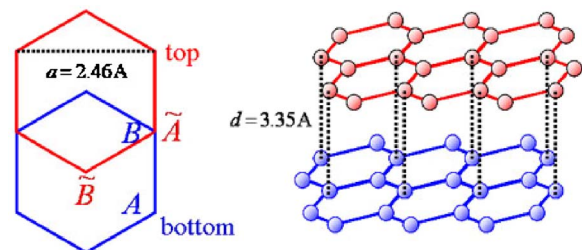

FIG. 1. (Color online) Structure of a graphene bilayer with honeycomb lattice constant $a=2.46$ Å and interlayer separation $d=3.35$ Å.
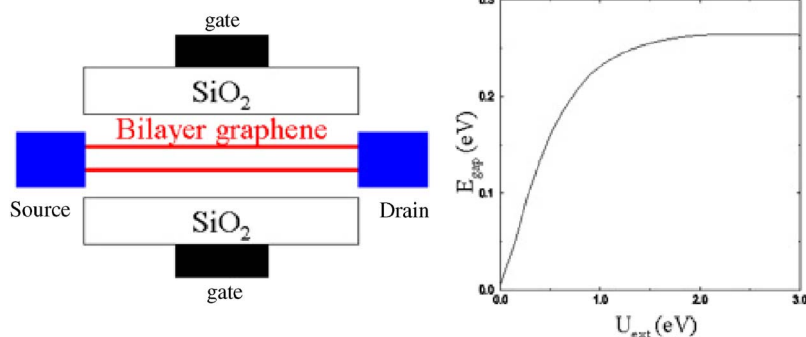
FIG. 2. (Color online) Schematic illustration of a circuit with a bilayer graphene channel sensitive to an external gate voltage. The graphene channel is separated from the front and back gates by a SiO$_2$ layer. The channel resistance change will be rapid and large when the graphene channel is undoped and isolated from the gate electrodes, as illustrated here. In this case, the total charge density in the bilayer system is fixed and the chemical potential lies in the gap opened by the gate voltage. This geometry could also be used to capacitively probe the correlation physics of the isolated bilayer system, as discussed in the text.

der to resolve the small gaps produced by small external fields, we performed BZ sums using a relatively large number of **k** points ($\sim$800) per irreducible wedge (5000 **k** points in the whole BZ). Total energies were convergent to within 0.0001 Ry.

Figure 3 shows the Coulomb potential relative to the Fermi energy, laterally averaged along a line in the *x-y* plane that includes an equal number of atoms in each layer, as a function of the *z* coordinate. The potential includes the Hartree electron-electron potential and the electron-ion interaction but not the external electric field potential or the exchange-correlation potential. The bilayer is centered around $z/z_0=0.25$, where z_0 is the superlattice period. (In the discussion below, we define the external potential energy U_{ext} as $U_{ext}=eE_{z,ext}d$, where $E_{z,ext}$ is an external electric field along the *z* direction and *d* is the interlayer separation of bilayer graphene which we take to be 3.35 Å.) In the absence of an electric field (dashed line), the Coulomb potential is flat
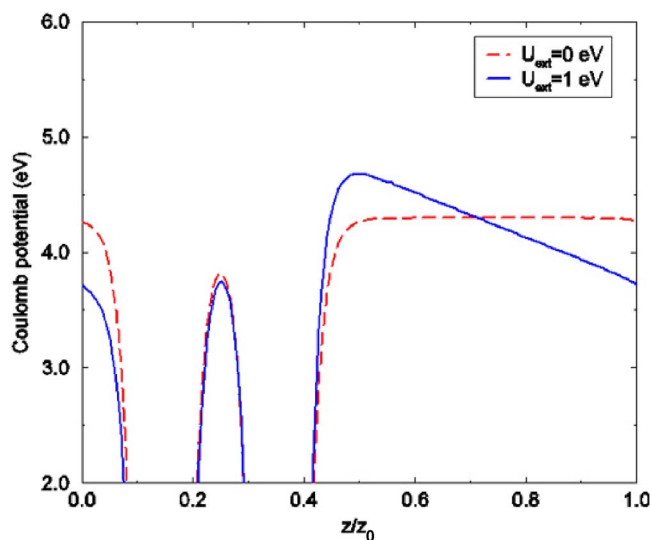

FIG. 3. (Color online) An averaged Coulomb potential of a cross section vs *z* for total external potential $U_{ext}=0$ eV and $U_{ext}=1$ eV. Here, z_0 is the superlattice period and the cross section was chosen to include equal number of atoms in each layer.

in the vacuum region and the energy difference between the vacuum and the Fermi energy gives estimates of the work function of bilayer graphene to be $\sim$4.3 eV. In the presence of an electric field (solid line), charge transfer between the layers induces a potential which cancels the external potential in the vacuum region. The difference between the Coulomb energies of the two layers in the presence of an external electric field is closely related to the gate-voltage induced energy gap.

B. Energy bands

Figure 4(a) shows the DFT energy band structure of bilayer graphene in the absence of an applied external electric field. When $U_{ext}=0$ eV, the low-energy band dispersion is nearly parabolic at two inequivalent corners, *K* and *K'*, of the hexagonal BZ, as predicted by the π-orbital tight-binding and continuum model phenomenologies.[11,12] The valence and conduction bands meet at the Fermi level.

In the absence of an external electric field, bilayer graphene, like single-layer graphene, is a zero-gap semiconductor. At finite U_{ext}, however, the low-energy bands near the *K* or *K'* point split, as explained in the Introduction. Therefore, gated graphene bilayer systems are gate-voltage tunable narrow gap semiconductors [Fig. 4(b)]. This property is unique, to our knowledge. It is worth noting that in the presence of an external electric field, the true energy gap does not occur at the *K* or *K'* point but slightly away from it. The low-energy spectrum develops a *Mexican hat* structure as the strength of the external electric field increases. This property is also captured by phenomenological models of graphene bilayers.[12]

C. Evolution of tight-binding model parameters with U_{ext}

Figure 5 illustrates DFT predictions for the evolution of tight-binding parameters with the applied external potential. The tight-binding model expression for the four low-energy band eigenvalues at the *K* and *K'* points is $E_{K/K'}=\pm U/2$, $\pm\sqrt{\gamma_1^2+U^2/4}$,[11] where *U* is the interlayer energy difference and γ_1 is the interlayer tunneling amplitude. (As we discuss
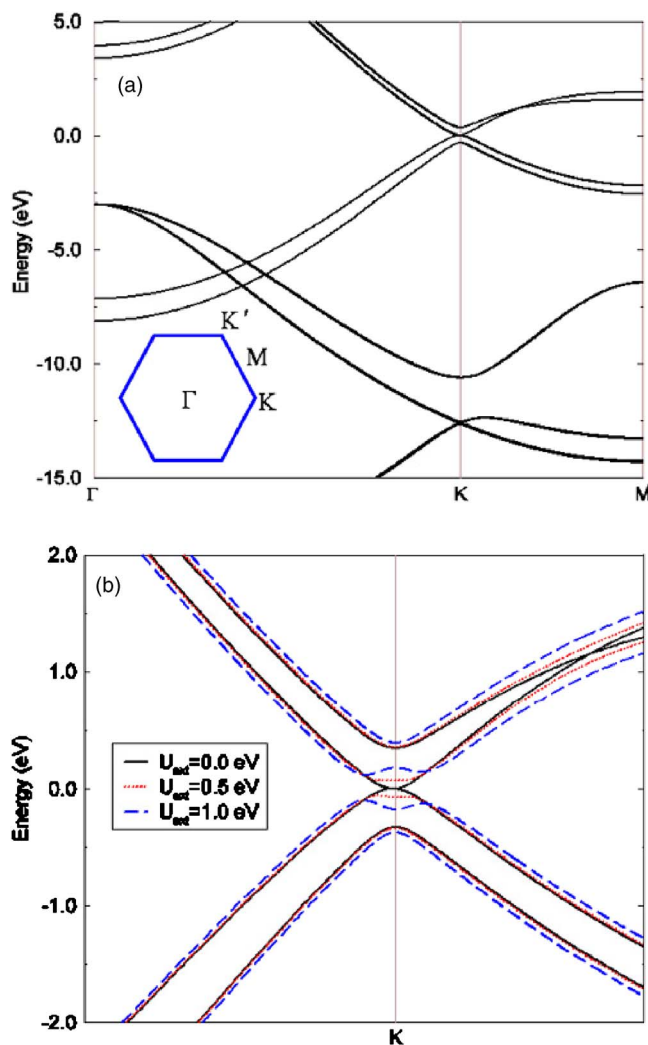
FIG. 4. (Color online) (a) Bilayer graphene band structure in the absence of an external electric field. (b) Bilayer graphene band structure near the K point for $U_{ext}=0$, 0.5, and 1 eV.
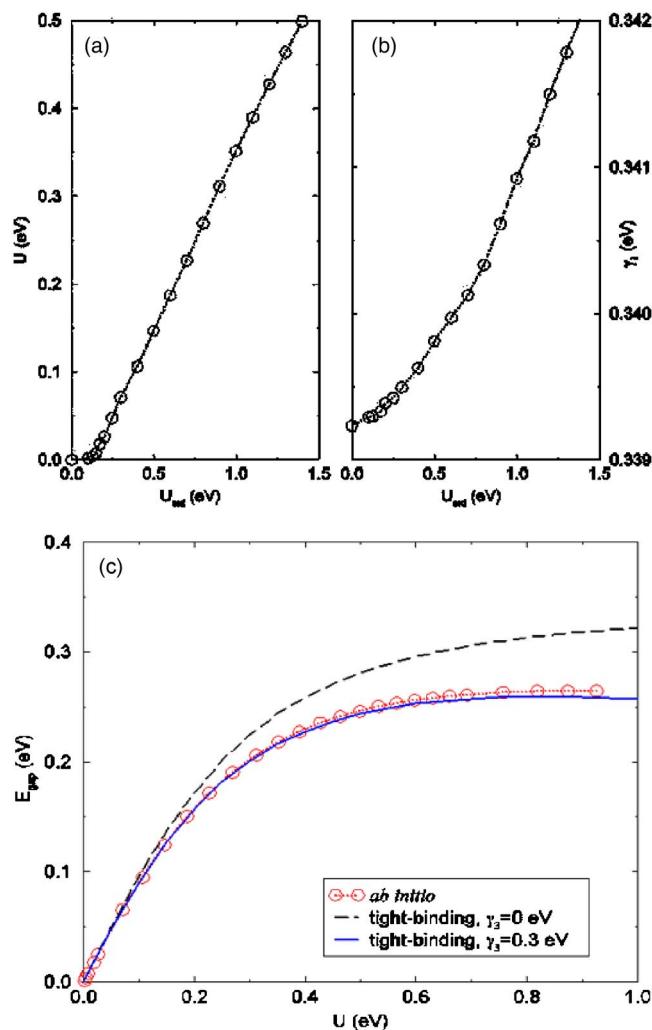

FIG. 5. (Color online) (a) Evolution of the graphene bilayer screened on-site energy difference U, extracted from the *ab initio* DFT bands as explained in the text, with the external potential U_{ext}. The external potential is strongly screened. (b) Evolution of the interlayer tunneling amplitude γ_1 with U_{ext}. (c) Comparison of band gap as a function of the on-site energy difference U obtained from the *ab initio* DFT calculations (open circles) with the tight-binding result for $\gamma_3=0$ (dashed line) and $\gamma_3=0.3$ eV (solid line).

below, this expression should, strictly speaking, be slightly modified in the presence of an external potential, but it still provides a convenient way of characterizing DFT predictions for the low-energy bands.) The values of U and γ_1 plotted in Fig. 5 represent this interpretation of the four lowest-energy DFT eigenvalues and clearly reflect substantial screening of the external interlayer potential by the Hartree potential plotted in Fig. 3. The interlayer coupling γ_1 increases monotonically as the external potential increases. The rate of increase is, however, ten times smaller than estimated in a recent experimental study[5] of a doped bilayer systems, possibly suggesting significant differences between doped and undoped systems. The intralayer nearest-neighbor π-electron hopping amplitude γ_0 and the interlayer A-$\tilde{B}$ coupling γ_3 were fitted to reproduce the band dispersion around the K/K' points at low energies. We find $\gamma_0 \approx 2.6$ eV and $\gamma_3 \approx 0.3$ eV, nearly independent of the external electric field. This value for γ_0 corresponds to an in-plane velocity $v = \frac{\sqrt{3}}{2}\frac{a\gamma_0}{\hbar} \approx 8.4 \times 10^5$ m/s, where the lattice constant $a=2.46$ Å.

Figure 5(c) compares the relationship between the on-site energy difference U extracted from the DFT calculations and

the energy gap with the corresponding relationship in the tight-binding model. Note that the gap does not increase indefinitely with U but saturates at ~ 0.3 eV due to the Mexican hat structure shown in the bands illustrated in Fig. 4. For $\gamma_3=0$, we can estimate the approximate energy gap from the low-energy approximation of the tight-binding model given by $E_{gap} \approx |U|\gamma_1/\sqrt{\gamma_1^2+U^2}$, where E_{gap} approaches $\gamma_1 \approx 0.34$ eV as U increases.[12] For $\gamma_3 \approx 0.3$ eV, however, E_{gap} is reduced from that of $\gamma_3=0$ and matches well with the DFT results. A nonzero value for γ_3 has a noticeable quantitative influence on the bands. This agreement confirms (unsurprisingly) that the tight-binding model captures the character of the low-energy bands in bilayer graphene. The most interesting physics is in the relationship between U and U_{ext}, which we now examine more closely.

III. SCREENING THEORIES

A. Continuum Hartree potential models

The screening of the external potential has been examined previously for both doped and undoped bilayers using phenomenological approaches combined with the Poisson equation.[12] This type of analysis provides a good reference point for interpreting the DFT results so we start with a discussion of this picture. Consider a graphene bilayer with an interlayer separation d under an external electric field $E_{z,ext}$ along the z direction. Neglecting the finite thickness and crystalline inhomogeneity of the graphene layers, and screening external to the bilayer, the Poisson equation is

$$\nabla \cdot \boldsymbol{E} = 4\pi(-e)[n_1 \delta(z) + n_2 \delta(z-d)], \quad (1)$$

where n_1 and n_2 are the net charge densities on the bottom and top layers, respectively. If the bilayer is placed on a gate dielectric such as silicon dioxide (SiO$_2$) and a voltage is applied between a gate and the bilayer, an excess charge carrier density $n = n_1 + n_2$ is supplied to the bilayer graphene and redistributed between the top and bottom layers due to an external electric field.

In order to compare with our DFT calculations, we focus here on the isolated bilayer case illustrated in Fig. 2, in which the total excess density $n = n_1 + n_2 = 0$. Let us define $\delta n = n_2 = -n_1$. From Eq. (1), we obtain the screened electric field E_z between the graphene sheets of the bilayer to be

$$E_z - E_{z,ext} = 4\pi e \delta n. \quad (2)$$

Adding the corresponding Hartree potential to the external potential, we obtain the screened interlayer potential difference as

$$U = U_{ext} + 4\pi e^2 d \delta n, \quad (3)$$

where $U = e E_z d$ and $U_{ext} = e E_{z,ext} d$.

To estimate the relationship between U and U_{ext}, we need only a theory for the dependence of δn on U. In the π-orbital tight-binding model, δn is given by the following integral over the BZ:

$$\delta n = \sum_{i \in occ} 2 \int_{BZ} \frac{d^2 k}{(2\pi)^2} \left\langle \psi_i(\boldsymbol{k}) \left| \frac{\sigma_z}{2} \right| \psi_i(\boldsymbol{k}) \right\rangle, \quad (4)$$

where $|\psi_i(\boldsymbol{k})\rangle$ is a band eigenstate in the presence of U, $\sigma_z = \text{diag}(1,1,-1,-1)$ in the (top, bottom) $\times (A,B)$ basis, and the index i runs over all occupied states. The factor of 2 was included to account for spin degeneracy.

Figure 6 compares the screening ratio U_{ext}/U obtained from the *ab initio* DFT calculations with the screening ratio from π-orbital tight-binding model self-consistent Hartree calculations with and without corrections that account for the crystalline inhomogeneity within each layer as explained later. The agreement between the three different approaches is generally good especially at large potentials.

Note that as U approaches zero, U_{ext}/U increases in all approximations. This property reflects increased screening as the gap decreases and is explained most succinctly using the two-band continuum model[11] for the lowest-energy bands:
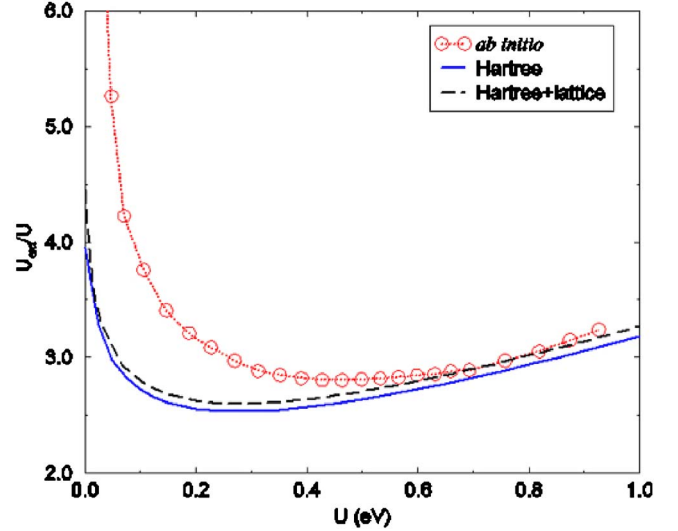

FIG. 6. (Color online) The ratio of the external electric potential U_{ext} to the interlayer energy difference inferred from the *ab initio* DFT calculation compared with the value of the same ratio in tight-binding model self-consistent Hartree calculations, both with and without crystalline inhomogeneity corrections. The tight-binding model calculations used $\gamma_0 = 2.6$ eV for the intralayer tunneling amplitude, $\gamma_1 = 0.34$ eV for the interlayer tunneling amplitude, and $\gamma_3 = 0.3$ eV for the interlayer A-$\tilde{B}$ coupling.

$$H_{eff} \approx \frac{U}{2} \begin{pmatrix} 1 & 0 \\ 0 & -1 \end{pmatrix} - \frac{1}{2m} \begin{pmatrix} 0 & (\pi^\dagger)^2 \\ \pi^2 & 0 \end{pmatrix} = \boldsymbol{a} \cdot \boldsymbol{\sigma}, \quad (5)$$

where $\pi = p_x + i p_y$, $m = \frac{\gamma_1}{2v^2}$, $\boldsymbol{a} = \left(-\frac{p_x^2 - p_y^2}{2m}, -\frac{p_x p_y}{m}, \frac{U}{2} \right)$, and $\boldsymbol{\sigma}$ are 2×2 Pauli matrices describing the top and bottom layer low-energy sites. This Hamiltonian has simple spectra $\epsilon_\pm = \pm|\boldsymbol{a}|$ with eigenfunctions given by

$$|+\rangle = \begin{pmatrix} \cos \frac{\theta}{2} e^{-i\phi/2} \\ \sin \frac{\theta}{2} e^{i\phi/2} \end{pmatrix}, \quad |-\rangle = \begin{pmatrix} -\sin \frac{\theta}{2} e^{-i\phi/2} \\ \cos \frac{\theta}{2} e^{i\phi/2} \end{pmatrix}, \quad (6)$$

where $\tan \theta = \frac{\sqrt{a_1^2 + a_2^2}}{a_3}$ and $\tan \phi = \frac{a_2}{a_1}$. It follows that

$$\begin{aligned} \delta n &= 4 \int_{|p| < p_c} \frac{d^2 p}{(2\pi\hbar)^2} \left\langle -, \boldsymbol{p} \left| \frac{\sigma_z}{2} \right| -, \boldsymbol{p} \right\rangle \\ &= -\frac{1}{\pi\hbar^2} \int_0^{p_c} p \, dp \cos\theta(\boldsymbol{p}) \\ &= -\frac{mU}{2\pi\hbar^2} \ln\left[x_c + \sqrt{x_c^2 + 1} \right], \end{aligned} \quad (7)$$

where $x_c = \frac{p_c^2}{mU}$. We have inserted a factor of 4 in this continuum model calculation to account for both spin ($\uparrow$ and $\downarrow$) and valley (K and K') degeneracies. The integral over wave vector was cut off at the radius $p_c \sim \sqrt{2m\gamma_1}$ beyond which the continuum model fails.

Inserting Eq. (7) in Eq. (3), we obtain

$$\frac{U_{ext}}{U} = 1 - 4\pi e^2 d \frac{\delta n}{U} = 1 + 2\left(\frac{d}{a_B}\right)\left(\frac{m}{m_e}\right)\ln[x_c + \sqrt{x_c^2 + 1}],$$

$$(8)$$

where $a_B = \hbar^2/m_e e^2$ is the Bohr radius and m_e is the bare electron mass. For small U, x_c is large and this simplifies to

$$\frac{U_{ext}}{U} \approx 2\left(\frac{d}{a_B}\right)\left(\frac{m}{m_e}\right)\ln\left[\frac{2p_c^2}{mU}\right].$$

$$(9)$$

A related observation concerning the logarithmic divergence of the screening ratio at small gate voltages was made previously by McCann.[12] All three of our calculations exhibit this increased screening at weak external potentials, with the largest upturn in the *ab initio* calculations.

B. Lattice Hartree potential models

We now turn our attention to one important contribution to discrepancies between the *ab initio* DFT results and the predictions of self-consistent Hartree models similar to those described above, the role of crystalline inhomogeneity in bilayer and single-layer graphene electrostatics. We consider a general two-body interaction term $\hat{V}$,

$$\hat{V} = \frac{1}{2}\sum_{\lambda_1',\lambda_2',\lambda_1,\lambda_2} \langle\lambda_1'\lambda_2'|V|\lambda_1\lambda_2\rangle c_{\lambda_1'}^\dagger c_{\lambda_2'}^\dagger c_{\lambda_2} c_{\lambda_1},$$

$$(10)$$

where $c_\lambda^\dagger$ and c_λ are creation and annihilation operators for a state λ. To capture the main consequences of crystalline inhomogeneity, we assume that the π-orbital Bloch states with crystal momentum $\boldsymbol{k}$ can be written as a linear combination of atomic orbitals,

$$\psi_{k,\lambda}(\boldsymbol{x}) = \frac{1}{\sqrt{N}}\sum_{\boldsymbol{R}} e^{ik\cdot R}\phi_\lambda(\boldsymbol{x} - \boldsymbol{R} - \tau_\lambda),$$

$$(11)$$

where ϕ_λ is an atomiclike π orbital, $\boldsymbol{R}$ is a lattice vector, τ_λ is the displacement of the sites in a unit cell with respect to the lattice vector, and N is the number of lattice sites. If we assume that the overlap of ϕ_λ orbitals centered on different sites can be neglected and ignore the $\hat{z}$ direction spread of the graphene sheets, the interaction Hamiltonian simplifies to

$$\hat{V} = \frac{1}{2\Omega}\sum_{k_1,k_2,q}\sum_{\lambda_1,\lambda_2} \widetilde{V}_{\lambda_1,\lambda_2}(\boldsymbol{q})c_{k_1+q,\lambda_1}^\dagger c_{k_2-q,\lambda_2}^\dagger c_{k_2,\lambda_2} c_{k_1,\lambda_1},$$

$$(12)$$

where Ω is the area of the two-dimensional plane,

$$\widetilde{V}_{\lambda_1,\lambda_2}(\boldsymbol{q}) = V_{\lambda_1,\lambda_2}(\boldsymbol{q})w_{\lambda_1}(-\boldsymbol{q})w_{\lambda_2}(\boldsymbol{q})e^{i\boldsymbol{q}\cdot(\tau_{\lambda_1}-\tau_{\lambda_2})}, \quad (13)$$

$$V_{\lambda_1,\lambda_2}(\boldsymbol{q}) = \int d\boldsymbol{x} e^{-i\boldsymbol{q}\cdot\boldsymbol{x}} V_{\lambda_1,\lambda_2}(\boldsymbol{x}), \quad (14)$$

and

$$w_\lambda(\boldsymbol{q}) = \int d\boldsymbol{x} e^{-i\boldsymbol{q}\cdot\boldsymbol{x}}|\phi_\lambda(\boldsymbol{x})|^2. \quad (15)$$

Note that the labels $\boldsymbol{k}_1$ and $\boldsymbol{k}_2$ are restricted to the BZ, while $\boldsymbol{q}$ runs over the two-dimensional plane. In Eq. (14),

$V_{\lambda_1,\lambda_2}(\boldsymbol{x}) = e^2/|\boldsymbol{x}|$ when λ_1 and λ_2 refer to sites in the same layer and $V_{\lambda_1,\lambda_2}(\boldsymbol{x}) = e^2/\sqrt{|\boldsymbol{x}|^2 + d^2}$ when λ_1 and λ_2 refer to layers separated by d. It follows that $V_{\lambda_1,\lambda_2}(\boldsymbol{q}) = 2\pi e^2/|\boldsymbol{q}|$ for labels in the same layer and $V_{\lambda_1,\lambda_2}(\boldsymbol{q}) = 2\pi e^2 \exp(-|\boldsymbol{q}|d)/|\boldsymbol{q}|$ for labels in different layers. Since the total charge of the bilayer is fixed in our calculations, only the differences between the various $\widetilde{V}_{\lambda_1,\lambda_2}(\boldsymbol{q})$ values are relevant. For explicit calculations, we have used a Gaussian form factor $w_\lambda(\boldsymbol{q}) = e^{-|\boldsymbol{q}|^2 r_0^2/2}$ corresponding to $|\phi_\lambda(\boldsymbol{x})|^2 \propto e^{-|\boldsymbol{x}|^2/2r_0^2}$, where $r_0 \sim 0.48$ Å was obtained by fitting to the DFT valence orbitals.

This two-body Hamiltonian can be used to account for crystalline inhomogeneity in a graphene bilayer system with arbitrary electronic correlations. To compare with the *ab initio* DFT calculations, we consider interactions in a mean-field Hartree approximation in which the interaction contribution to the single-particle Hamiltonian is

$$\hat{V}^{(H)} = \sum_{k,a,\sigma} \epsilon_{a\sigma}^{(H)} c_{k,a\sigma}^\dagger c_{k,a\sigma,} \quad (16)$$

where a and σ denote layer and sublattice degrees of freedom. Here,

$$\epsilon_{a\sigma}^{(H)} = \sum_{a',\sigma'} \widetilde{V}_{a\sigma,a'\sigma'} n_{a'\sigma'}, \quad (17)$$

where $n_{a\sigma} = \frac{2}{\Omega}\sum_k \langle c_{k,a\sigma}^\dagger c_{k,a\sigma}\rangle$ including spin degeneracy and

$$\widetilde{V}_{a\sigma,a'\sigma'} = \sum_G \widetilde{V}_{a\sigma,a'\sigma'}(\boldsymbol{G}), \quad (18)$$

with $\boldsymbol{G}$ a triangular lattice reciprocal-lattice vector.

As explained in the Introduction, interlayer tunneling in graphene leads to high-energy bands which favor the $\widetilde{A}$-B sites and low-energy bands that favor the A-$\widetilde{B}$ sites. Since the low-energy bands respond most strongly to the external potential, we can expect that the charge transfer occurs more strongly on the A-$\widetilde{B}$ sites, and that the screening potential should be larger on these sites. Instead of a single-interlayer Hartree screening potential, two Hartree potentials for low and high bands must be calculated separately:

$$\epsilon_l^{(H)} = \epsilon_{\widetilde{B}}^{(H)} - \epsilon_A^{(H)},$$

$$\epsilon_h^{(H)} = \epsilon_{\widetilde{A}}^{(H)} - \epsilon_B^{(H)}. \quad (19)$$

When only the $\boldsymbol{G} = 0$ term is retained in the reciprocal-lattice vector sum,

$$\epsilon_l^{(H0)} = \epsilon_h^{(H0)} = 2\pi e^2 d(n_{\widetilde{A}} + n_{\widetilde{B}} - n_A - n_B), \quad (20)$$

and Eq. (3) is recovered.

It turns out that the sum over reciprocal-lattice vectors can be truncated with good accuracy at the first shell. Noting that $e^{-|G|d} \ll 1$, we find for the crystalline inhomogeneity corrections

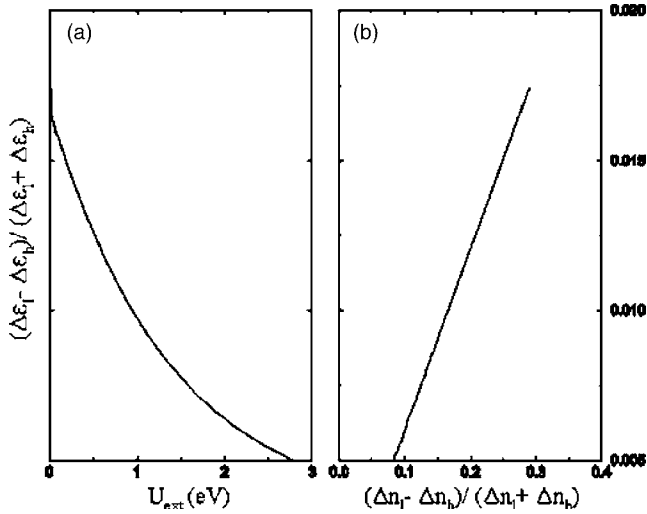$$\epsilon_l^{(H1)} \approx 2\pi e^2 d\alpha(\boldsymbol{G})(6\Delta n_l - 3\Delta n_h),$$

FIG. 7. Splitting of Hartree potentials $(\epsilon_l^{(H)} - \epsilon_h^{(H)})/(\epsilon_l^{(H)} + \epsilon_h^{(H)})$ as a function of (a) the external electric potential U_{ext} and (b) the corresponding density inhomogeneity $(\Delta n_l - \Delta n_h)/(\Delta n_l + \Delta n_h)$ in the lattice Hartree potential model.

$$\epsilon_h^{(H1)} \approx 2\pi e^2 d\alpha(\boldsymbol{G})(6\Delta n_h - 3\Delta n_l), \tag{21}$$

where $\Delta n_l = n_{\tilde{B}} - n_A$, $\Delta n_h = n_{\tilde{A}} - n_B$, and $\alpha(\boldsymbol{G}) = e^{-|G|^2 r_0^2}/|G|d \approx 0.0136$. Thus, the inhomogeneity effect results in more screening as expected, but as indicated by the black dashed line in Fig. 6, it is not able to account for the largest part of the discrepancy between DFT and model results.

As the external electric potential is decreased, the difference between low-energy and high-energy site occupancies is increased. The difference in Hartree potentials rises correspondingly, as illustrated in Fig. 7(a). From Eq. (21), we can estimate the relation between the splitting of the Hartree potentials and the density inhomogeneity:

$$\frac{\epsilon_l^{(H)} - \epsilon_h^{(H)}}{\epsilon_l^{(H)} + \epsilon_h^{(H)}} \approx \frac{9}{2}\alpha(\boldsymbol{G})\frac{\Delta n_l - \Delta n_h}{\Delta n_l + \Delta n_h}, \tag{22}$$

where the coefficient $\frac{9}{2}\alpha(\boldsymbol{G})$ is given by ~ 0.0612 [Fig. 7(b)].

IV. DISCUSSION

Our DFT calculations of external potential induced gaps in the electronic structure of graphene bilayers confirm the simple picture provided by phenomenological tight-binding models. The *ab initio* calculations include a number of effects not contained in the model calculations. For example,

the occupied σ orbitals within each graphene plane, which are neglected in the π-orbital tight-binding model, will be slightly polarized by the external electric field and contribute to screening. In the DFT calculations, not only Hartree potentials but also exchange-correlation potentials will be altered by an external electric field and influence the screening process. Since the exchange potential is attractive, its contribution to the total potential will lower energies in a layer more as the density is increased. The exchange potential therefore makes a negative contribution to the screening ratio. The quantitative discrepancies between the DFT and phenomenological model reflect the combination of these and other additional effects contained in the DFT calculations, and strong sensitivity to intralayer and interlayer tunneling amplitudes which may not be evaluated with perfect accuracy by DFT. We also note that the low-energy eigenstates in bilayer graphene are coherent combinations of amplitudes on both layers, which implies that interlayer exchange interactions will be substantial. This kind of effect is absent in the exchange-correlation potentials commonly used in DFT. Indeed, it is entirely possible that DFT calculations do not predict accurate values for the screening ratio. We believe that there is strong motivation for capacitive studies of the interlayer screening properties of graphene bilayers using an experimental arrangement similar to that in Fig. 2.

In summary, we have used *ab initio* density functional theory calculations to study the gate-voltage tunable gap in the electronic structure of bilayer graphene. The electric-field dependence of the on-site energy difference and the interlayer tunneling amplitude were extracted from the DFT calculation results by fitting to tight-binding model expressions for high-symmetry point graphene bilayer band eigenvalues. The screening effect seen in the DFT calculations can be explained by a tight-binding model self-consistent Hartree method including crystalline inhomogeneity corrections, although the DFT screening is stronger especially for weak external potentials.

---

*Electronic address: hongki@physics.utexas.edu

[1] K. S. Novoselov, A. K. Geim, S. V. Morozov, D. Jiang, Y. Zhang, S. V. Dubonos, I. V. Grigorieva, and A. A. Firsov, Science **306**, 666 (2004).

[2] K. S. Novoselov, D. Jiang, F. Schedin, T. J. Booth, V. V. Khotkevich, S. V. Morozov, and A. K. Geim, Proc. Natl. Acad. Sci.

U.S.A. **102**, 10451 (2005).

[3] Y. Zhang, Joshua P. Small, Michael E. S. Amori, and Philip Kim, Phys. Rev. Lett. **94**, 176803 (2005).

[4] K. S. Novoselov, E. McCann, S. V. Morozov, V. I. Fal'ko, M. I. Katsnelson, U. Zeitler, D. Jiang, F. Schedin, and A. K. Geim, Nat. Phys. **2**, 177 (2006).

[5] Taisuke Ohta, Aaron Bostwick, Thomas Seyller, Karsten Horn, and Eli Rotenberg, Science **313**, 951 (2006).

[6] K. S. Novoselov, A. K. Geim, S. V. Morozov, D. Jiang, M. I. Katsnelson, I. V. Grigorieva, S. V. Dubonos, and A. A. Firsov, Nature (London) **438**, 197 (2005).

[7] Y. Zhang, Yan-Wen Tan, Horst L. Stormer, and Philip Kim, Nature (London) **438**, 201 (2005).

[8] C. L. Kane and E. J. Mele, Phys. Rev. Lett. **95**, 226801 (2005); **95**, 146802 (2005).

[9] N. A. Sinitsyn, J. E. Hill, Hongki Min, Jairo Sinova, and A. H. MacDonald, Phys. Rev. Lett. **97**, 106804 (2006); Hongki Min, J. E. Hill, N. A. Sinitsyn, B. R. Sahu, Leonard Kleinman, and A. H. MacDonald, Phys. Rev. B **74**, 165310 (2006).

[10] Sylvain Latil and Luc Henrard, Phys. Rev. Lett. **97**, 036803 (2006); B. Partoens and F. M. Peeters, Phys. Rev. B **74**, 075404 (2006).

[11] Edward McCann and Vladimir I. Fal'ko, Phys. Rev. Lett. **96**, 086805 (2006).

[12] Edward McCann, Phys. Rev. B **74**, 161403(R) (2006).

[13] Eduardo V. Castro, K. S. Novoselov, S. V. Morozov, N. M. R. Peres, J. M. B. Lopes dos Santos, Johan Nilsson, F. Guinea, A. K. Geim, and A. H. Castro Neto, cond-mat/0611342 (unpublished).

[14] W. Kohn and L. J. Sham, Phys. Rev. **140**, A1133 (1965).

[15] P. Blaha, K. Schwarz, G. K. H. Madsen, D. Kvasnicka, and J. Luitz, *WIEN2K, An Augmented Plane Wave+Local Orbitals Program for Calculating Crystal Properties*, edited by K. Schwarz (Technische Universität Wien, Vienna, Austria, 2001).

[16] J. P. Perdew, K. Burke, and M. Ernzerhof, Phys. Rev. Lett. **77**, 3865 (1996).

[17] J. Stahn, U. Pietsch, P. Blaha, and K. Schwarz, Phys. Rev. B **63**, 165205 (2001).